Environmental Factors Contributing to Tropical Cyclone Genesis over the Western North Pacific

RYUJI YOSHIDA AND HIROHIKO ISHIKAWA

Disaster Prevention Research Institute, Kyoto University, Uji, Kyoto, Japan

(Manuscript received 28 October 2011, in final form 18 July 2012)

ABSTRACT

The flow environment associated with tropical cyclone genesis (TCG) over the western North Pacific was assessed via categorization into five flow patterns: monsoon shear line (SL), monsoon confluence region (CR), monsoon gyre (GY), easterly wave (EW), and preexisting tropical cyclone (PTC). Using reanalysis data and an objective algorithm, the authors defined ''contribution scores'' for the five flow patterns. Each score represents the contribution to TCG from each flow pattern, and scores were calculated for 908 TCG cases from 1979 to 2008 (30 yr). Of the major contribution flow patterns, SL accounted for 42% of TCGs, EW for 18%, CR for 16%, PTC for 11%, and GY for 6%. Seasonal variations in the occurrence frequency of these five patterns were clear, but interannual variations were not as apparent. Tropical cyclones often appear to be generated in conditions with multiple flow patterns. Thus, relationships between multiple flow patterns were investigated by comparing contribution scores. The SL and CR patterns were strongly correlated to each other, which can be explained by the monsoon southwesterly that organizes both patterns. The EW pattern tends to be independent of the other flow patterns. The PTC pattern has a relatively high correlation with CR, but does not have a correlation with SL or EW. Thus, the characteristics of flow patterns for the occurrence frequency of TCG are derived for a longer period than in previous studies, and correlations among flow patterns are also investigated.

1. Introduction

This study aims to expand upon previous studies to develop the understanding of tropical cyclone genesis in the western North Pacific over a multidecadal time frame. Several studies of the preferred synoptic conditions for the genesis and development of tropical cyclones (TCs) have been made. Gray (1968, 1998) considered environmental factors such as high sea surface temperature, conditional instability, and high relative humidity in the midtroposphere, cyclonic absolute vorticity in the lower troposphere, anticyclonic absolute vorticity in the upper troposphere, and weak vertical shear of horizontal wind as providing the preferred environment for tropical cyclone genesis (TCG). Research on the tropospheric dynamical conditions for TCG include Zehr (1992) and Ritchie and Holland (1999, hereafter RH99), both over the western North Pacific (WNP). Zehr (1992) investigated the environment flow for TCGs associated with the monsoon trough. He classified such TCGs into prominent easterly, weak westerly, and strong westerly patterns. RH99 considered five environmental flow patterns preferred for TCG: monsoon shear line (SL), monsoon confluence region (CR), monsoon gyre (GY), easterly wave (EW), and Rossby wave energy dispersion (RD). Of these five patterns, the SL, CR, and GY patterns are related to the monsoon trough. Gray (1968, 1998) mentioned that the monsoon trough is the most favorable environment for the formation of multiday persistent cloud clusters that frequently grow into TCs. The trough extends from the Indochina Peninsula in the west to the east of the Philippine Sea, and is accompanied by southwesterly flow on its southern side. The SL, CR, and GY patterns have different kinematic features. The SL pattern involves cyclonic shear of the horizontal wind along the monsoon trough. The CR pattern is the confluence zone between monsoon westerly and easterly winds (RH99). Holland (1995) suggested that equatorial waves become trapped in the CR, and that the waves intensify. This can lead to an accumulation of wave energy in the region, and increased potential for cyclogenesis. The GY

Corresponding author address: Ryuji Yoshida, Disaster Prevention Research Institute, Kyoto University, Gokasho, Uji, Kyoto 611-0011.
E-mail: yoshida@storm.dpri.kyoto-u.ac.jp

DOI: 10.1175/MWR-D-11-00309.1

pattern is a synoptic-scale gyre embedded within the monsoon trough (Lander 1994; Chen et al. 1996), which is formed when the strong shear flow of the monsoon trough is perturbed by easterly waves (Chen et al. 2008). Lander (1994) showed cases where several TCs were organized in association with a single monsoon gyre event persisting for several weeks over the WNP in 1991 and 1993.

The EW is a synoptic-scale wave within the trade wind system. The troughs of the EW are recognized as preferred environments for TCG over the equatorial Atlantic (Yanai 1961, 1968; Shapiro 1977). The EW trough sometimes develops into TCs in the equatorial Pacific (Heta 1990, 1991). Chen et al. (2008) also suggested that many TCGs over the WNP are affected by easterly waves.

The RD pattern is associated with a preexisting tropical cyclone (PTC; referred to as such in this study). A mature TC disperses its energy as a Rossby wave, which is emitted southeastward from the TC and forms a wave train. One of the low pressure areas of the wave train sometimes develops into a TC (McDonald 1998; Li and Fu 2006; Li et al. 2006).

RH99 categorized 199 TCGs from 1984 to 1992 (except 1989) into these five patterns using grid fields from the Australian Bureau of Meteorology tropical analysis scheme and Japanese Geostationary Meteorological Satellite images. They found that the percentage occurrence of TCG events attributable to the SL, CR, EW, RD, and GY patterns are 42%, 29%, 18%, 8%, and 3%, respectively. They also investigated the flow features of composited patterns for each category.

Lee et al. (2008, hereafter L08) have also investigated flow conditions over the WNP. They used meteorological geostationary satellite data and Quick Scatterometer (QuikSCAT) oceanic wind data and examined 124 TCG cases during the period from 1999 to 2004. They identified six flow patterns; the EW, SL, and CR patterns are the same as in RH99, but they introduced more localized flow patterns: northeasterly flow, coexistence of northeasterly and southwesterly flow, and southwesterly flow.

This study seeks to expand the time series of TCG analysis from periods of 8 (RH99) or 6 yr (L08), to 30 yr (from 1979 to 2008). A similar analysis over a longer period is required to investigate the existence of interannual change. Further, the past studies attributed each TCG event to a single flow pattern. Li and Fu (2006) intensively examined TCG associated with the PTC pattern, and reported cases where no TCG occurred despite a significant Rossby wave train. This finding suggests that some other background dynamic conditions are in operation. Since it is probable that several flow patterns contribute to a TCG case, the second and subsequent contributing patterns to each TCG event are considered in this study.

In contrast to the subjective classification procedures of RH99 and L08, this study employs an objective method to classify distinguishing patterns of the flow fields over the WNP. In the method, we first compute scores describing the contributions from the five different flow patterns to each TCG case. The flow pattern with the highest score is determined to be the dominant pattern. The second and the third contributions from other flow patterns are then examined using the minor scores. The flow patterns considered in this study are the five identified by RH99: the SL, CR, GY, EW, and PTC patterns.

In sections 2 and 3, the data and analysis method are explained, respectively. The results for the major contributions are analyzed in section 4a. In section 4b, we analyze the seasonal and interannual changes of the major contributions. The conditions of the upper troposphere are considered in section 4c. Relationships among the five flow patterns are discussed in section 5a. The TCG and the genesis potential index are compared in the light of environment flow pattern in section 5b. Finally, we show some examples of the unclassified cases in the present analysis in section 5c.

2. Data

The TCGs are taken from the best-track data of the Joint Typhoon Warning Center (JTWC) from 1979 to 2008. Of the 909 best-track records in the WNP basin in this period, 908 records are subject to analysis. The first record in January 1979 was excluded because the initial time of the TC fell outside of the data period.

Since we are interested in the early phase of TCG, the initial position and time of each best-track record are used as the place and time of TCG following RH99 and L08. In the present study, we use the 6-hourly reanalysis data produced by Japan Meteorological Agency (JMA): Japanese 25-yr Reanalysis (JRA-25)/JMA Climate Data Assimilation System (JCDAS; Onogi et al. 2007). The JRA-25 reanalysis project was conducted over 1979 to 2004, and the same reanalysis is being continued after 2005 using JCDAS algorithm. We used 30-yr data from 1979 to 2008. The horizontal resolution of the JRA-25/JCDAS data is 1.25°. For each TCG case, we compute five scores representing the contribution from the five flow patterns—SL, CR, GY, EW, and PTC (shown in Fig. 1)—using the reanalysis data.

RH99 showed that a precursor perturbation of TC appears approximately 72 h prior to the time of TCG for these patterns. Briegel and Frank (1997) also suggested

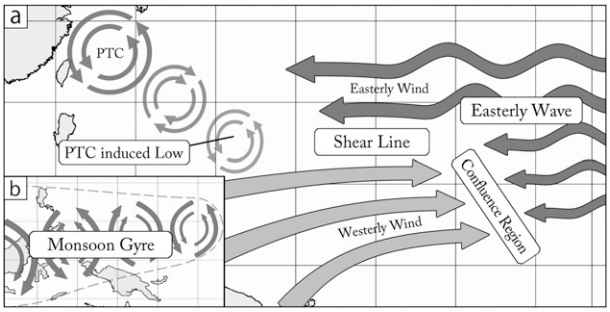

FIG. 1. A schematic image of the five flow patterns contributing to TCG based on RH99. The westerly and easterly winds are indicated by arrows, and a preexisting TC is indicated as a vortex shape.

that southwesterly surges that organize SL and CR occurred approximately 72 h prior to the TCG over the WNP. Considering these studies, we compute an averaged field from those taken 66 and 72 h before the TCG time, and compute contribution scores from SL, CR, GY, and EW. The averaging is applied to filter out small-scale perturbations. The 850-hPa wind is used in these scores. For the PTC pattern, the sea level pressure at the TCG time is used, because the wave train seen in the PTC pattern becomes significant at the time of TCG (RH99).

3. Definitions of contribution scores

In this section, the definition of five contribution scores and the detail calculation procedure are described.

a. The shear line pattern

As illustrated in Fig. 1, the SL is defined as a line-shaped region that has a horizontal wind shear of zonal component. The SL contribution to TCG is evaluated using the wind shear intensity and the distance between the location of TCG and SL. Thus, the score of SL is calculated by

$$\mathrm{SCR}_{\mathrm{SL}} = \frac{A\left(\dfrac{\partial u}{\partial y}\right)_{\mathrm{ave}} \exp(B \times \mathrm{dist})}{\mathrm{Max}[\mathrm{scr}_{\mathrm{SL}}]}. \qquad (1)$$

In this equation A and B are arbitrary constants and are set to $A = -1.0$ and $B = -1.0 \times 10^{-5}$. These constants are used to properly disperse $\mathrm{SCL}_{\mathrm{SL}}$ values for all cases across a wide range, and the detail is explained in section 3f. The raw contribution scores, $\mathrm{scr}_{\mathrm{SL}}$, are computed by $A(\partial u/\partial y)_{\mathrm{ave}} \times \exp(B \times \mathrm{dist}_{\mathrm{n}})$, which are then normalized by their maximum value, $\mathrm{Max}[\mathrm{scr}_{\mathrm{SL}}]$.

The location of SL at a fixed longitude is identified as the place where the sign of the zonal wind component changes from negative on the northern side of the grid to positive on the southern side. We first search for the SL

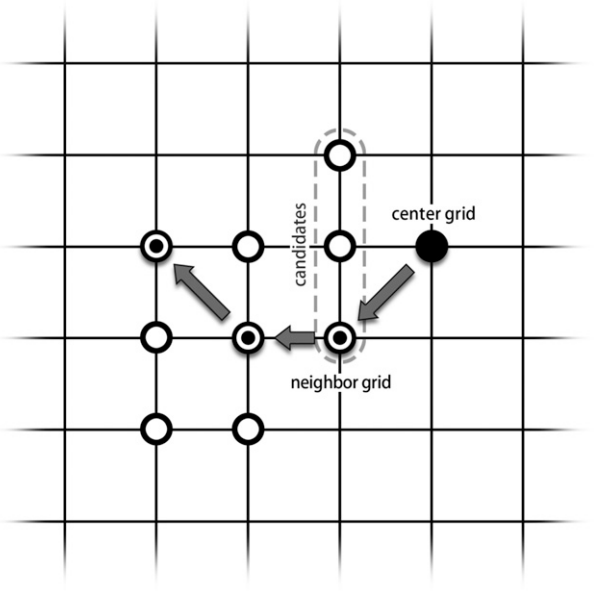

FIG. 2. An example of searching for a line-shaped region (i.e., SL or CR). The grids correspond to a latitude–longitude field, and have horizontal wind component data at each grid point. First, the center grid is defined as the location closest to the TCG at which the latitudinal shear of the zonal wind changes sign. Then, the neighboring grids are searched for a change in sign of the horizontal shear of the zonal wind. The neighboring grid cells are selected from each set of three candidate grids using the criteria, which are the boundary of the zonal wind, and a larger gradient of wind component than other candidates. Finally, the grid points defining the line shape region are selected following the gray arrows.

in the meridional direction at the longitude of TCG. If there are multiple grid cells satisfying the criteria, the one nearest to the TCG location is selected and called the ''center grid.'' The distance between the center grid and the TCG location is used as ''dist'' in Eq. (1). An upper limit of 1500 km is set for dist, since a SL far from the TCG location may not contribute to TCG. If the dist is more than 1500 km, the SL score is not calculated.

Next, we trace the shear line in the longitudinal direction from the center grid. At the neighboring longitudinal grid cells, the location of SL is searched for in the same manner as described above (see Fig. 2). In cases where multiple candidates exist, the location with the greatest gradient is selected. This procedure is repeated in the westward and the eastward directions until no more candidates are found. When the detected SL is shorter than six grid cells in the west–east direction, we assume that the SL is too short in length for TCG, and the SL score is not calculated. The intensity of the SL feature is calculated as the averaged meridional gradient of zonal wind over the detected SL. In the averaging, SL points more than 10 grid cells from the center grid are eliminated, if they exist.

b. The confluence region pattern

The CR is defined as the border between westerly and easterly winds, and its score is evaluated using the intensity of the zonal wind convergence and the distance between the location of TCG and calculated by

$$\mathrm{SCR}_{\mathrm{CR}} = \frac{A\left(\frac{\partial u}{\partial x}\right)_{\mathrm{ave}} \exp(B \times \mathrm{dist})}{\mathrm{Max}[\mathrm{scr}_{\mathrm{CR}}]}. \quad (2)$$

In this equation A and B are arbitrary constants, with $A = -1.0$ and $B = -1.0 \times 10^{-5}$. The values are normalized by their maxima, which are similar to that of the SL.

We first search for the grid where a westerly wind exists at the longitude of the TCG in the meridional direction. If there are multiple candidates, the location with the strongest wind speed is selected, and referred to as the ''westerly grid.'' If there is no westerly grid at the longitude of the TCG location, we search at a longitude one grid to the west. This is repeated until a candidate is found, or longitude is 70°E. If no candidate is found before 70°E, we do not calculate a CR score.

Once a westerly grid is identified, we search for the confluence of the zonal wind in a longitudinal direction at the latitude of the westerly grid. This confluence is detected as the grid cell where the sign of the zonal wind component changes from positive (western side) to negative (eastern side). If there are multiple candidates satisfying this criterion, the one nearest to the westerly grid is selected, and called the center grid. The distance between the TCG location and the center grid is calculated as dist in Eq. (2). We set an upper limit of 1500 km for dist since a CR far from the TCG location may not contribute to the genesis. If the dist is more than 1500 km, we do not calculate a CR score.

Next, we trace the CR from the center grid in the meridional direction. The location of CR is searched for in the same manner as SL, but the search direction is north–south. When the detected CR is shorter than three grid cells in the west–east direction, we assume that the CR is too short in length for TCG, and the CR score is not calculated. The intensity of the CR feature is calculated as the averaged longitudinal gradient of the zonal wind over the detected CR. In the averaging, CR points farther than six grid cells from the center grid are eliminated.

c. The easterly wave pattern

The EW contribution to TCG is evaluated using the intensity of the west–east shear of the meridional wind near the trough and the distance between the location of TCG and the trough. Thus, the contribution score for the EW pattern is calculated from the following equation:

$$\mathrm{SCR}_{\mathrm{EW}} = \frac{A\left(\frac{\partial v}{\partial x}\right) \exp(B \times \mathrm{dist})}{\mathrm{Max}[\mathrm{scr}_{\mathrm{EW}}]}, \quad (3)$$

where $A = 2.0 \times 10^{-1}$ and $B = -1.0 \times 10^{-2}$. The EW score is calculated only for cases when the TCG took place in easterly winds. We search for troughs of the easterly wave in a test domain, whose western edge is four grid cells to the west of the TCG location, and the eastern edge is 180°. The north–south width of the test domain is 11 grid cells centered at the TCG latitude. The trough is detected as the location where the meridional wind is northward to the east and southward to the west. That is, the sign of the meridional wind component is positive on the eastern side and negative on the western side, and is referred to as the ''trough grid''.

The distance between the trough grid and the TCG location is determined considering the movement of the trough. Since the meteorological field is taken as an average of 66 and 72 h before the TCG time, the westward propagation of the trough over a nominal 69 h must be considered. There are several discussions on the propagation speed of the easterly wave. The propagation speed of waves with a wavelength of 3000–4000 km is -9 m s^{-1} (Reed and Recker 1971), and that of wave with a wavelength of 4000 km is -11.6 m s^{-1} over the North Pacific (Serra et al. 2008). According to Tam and Li (2006), the shorter the wavelength, the slower the propagation speed to the west of 150°E. The zonal wind speed over the North Pacific is more than -8 m s^{-1} at its maximum, and tends to be much slower than the maximum over the western North Pacific (Serra et al. 2008). Considering this information, the propagation speed of the easterly wave is assumed to be the same as the averaged easterly wind speed near the trough. If there are multiple trough grids, the one nearest to the TCG location is selected. The distance of the nearest trough grid to the TCG location is used as dist in Eq. (3). The intensity of the EW feature is calculated as the longitudinal gradient of the meridional wind at the nearest trough grid.

d. The monsoon gyre pattern

The score of the GY pattern is evaluated using the similarity of the 850-hPa flow field to a composite of typical GY cases reported by Lander (1994). To calculate the GY score, a model GY pattern is first constructed. The model pattern is a composite of 6 TCG cases identified as the GY pattern by Lander (1994); these cases are the 10th (Ellie), 11th (Gladys), and 13th

(no name) TC records in 1991, and the 10th (Nathan), 11th (Ofelia), and 12th (Percy) TC records in 1993 in the JTWC best-track dataset. The score for the monsoon gyre pattern GY is calculated by

$$\mathrm{SCR}_{\mathrm{GY}} = \frac{\exp(-M) \times (\zeta - \zeta_{\mathrm{std}})}{\mathrm{Max}[\mathrm{scr}_{\mathrm{GY}}]}. \tag{4}$$

Vorticity ζ is calculated using the 850-hPa wind component at the TCG location. The vorticity is expressed as an excess from a standard value, $\zeta_{\mathrm{std}} = 1 \times 10^{-5}$, considering a discussion in RH99. According to RH99, the monsoon gyre has stronger low-level cyclonic vorticity ($\sim 2 \times 10^{-5}$ s^{-1}) than the shear line, so that the degree of excess from the standard should be used to represent the intensity of the GY pattern. In Eq. (4), M represents the degree of pattern matching between the model cases and the TCG case. M is calculated by

$$M = \sum_{i=0}^{ni} \sum_{j=0}^{nj} \sqrt{[C'_{(i,j)} - \mathrm{data}'_{(i,j)}]^2}, \tag{5}$$

where i and j represent the horizontal grid; ni and nj are the width and length, respectively, of the pattern matching test domain; C' is the model GY pattern sea level pressure (SLP) field; and data$'$ is the corresponding SLP field of a given TCG case. Prime means deviation from the average over the matching domain. If the TCG case is a good match to the model case, the degree of pattern matching "M" has a small value, and thus exp $(-1 \times M)$ has a large value.

e. The preexisting tropical cyclone pattern

Li and Fu (2006) and Li et al. (2006) analyzed PTC patterns in the horizontal wind at 850 hPa or surface pressure between the TCG location and PTC. Based on their discussion, the contribution score of PTC is estimated by the amplitude of the closest wave to the PTC, C_{wv1}, as

$$\mathrm{SCR}_{\mathrm{PTC}} = \frac{C_{wv1}^2}{\mathrm{Max}[\mathrm{scr}_{\mathrm{PTC}}]}. \tag{6}$$

Before calculation of the score, we search for PTC at the TCG time in the JTWC best-track data. Since the Rossby wave is emitted in the southeast direction from the PTC location, a PTC is identified only when it exists in the quadrant northwest of the TCG location. If there are multiple PTC candidates, the one closest to the TCG location is selected. Once a PTC is found, we compute the amplitude of the first Fourier component, C_{wv1}, of SLP along the line connecting the PTC and TCG locations. It should be noted that for the PTC score, the meteorological field at the TCG time is used instead of that 69 h before TCG.

TABLE 1. Examples of contribution scores of each of the five flow pattern calculated by the objective algorithm for some TCG cases in 1996. Bold characters indicate the maximum score in the TCG, thus the flow pattern with this score is identified as the major contribution.

TCG	Genesis time	SL	CR	GY	EW	PTC
D199601	0600 UTC 23 Feb 1996	**0.314**	0.000	0.004	0.311	0.000
D199602	1800 UTC 29 Mar 1996	**0.384**	0.000	0.146	0.092	0.000
D199603	0000 UTC 25 Apr 1996	0.232	0.000	0.000	**0.239**	0.000
D199604	0000 UTC 7 May 1996	0.099	**0.293**	0.091	0.036	0.000
D199605	0000 UTC 16 May 1996	0.000	0.000	0.000	0.000	0.000
D199606	1200 UTC 3 Jul 1996	0.000	0.000	0.000	0.000	0.000
D199607	0600 UTC 10 Jul 1996	0.000	**0.446**	0.000	0.000	0.393
D199608	1200 UTC 19 Jul 1996	**0.170**	0.000	0.000	0.000	0.000
D199609	0000 UTC 19 Jul 1996	0.000	**0.969**	0.000	0.383	0.263
D199610	0600 UTC 21 Jul 1996	0.000	0.000	0.000	0.073	**0.521**
D199611	0600 UTC 27 Jul 1996	**0.294**	0.000	0.000	0.000	0.037
D199612	1200 UTC 25 Jul 1996	0.000	0.336	0.000	0.037	**0.777**
D199613	0000 UTC 28 Jul 1996	**0.359**	0.211	0.000	0.012	0.139
D199614	0000 UTC 4 Aug 1996	**0.266**	0.000	0.000	0.000	0.000
D199615	0600 UTC 10 Aug 1996	0.178	0.000	0.483	**0.920**	0.000

f. The brief feature of scoring equations

Via calculations in the prior section, we obtain a set of normalized contribution scores from the five patterns for every TCG case. Table 1 shows examples of calculated contribution scores for some TCG cases in 1996. The maximum contribution score is shown in bold and the corresponding flow pattern is determined as the major flow pattern contributing to the TCG. The flow pattern of the next largest contribution score is assumed as the secondary contribution and so on. Figure 3 shows histograms of the calculated scores for five patterns over the 30-yr analysis period, and an example of tuning for arbitrary scaling factor in the SL pattern case.

To show the sensitivity of $\mathrm{SCL}_{\mathrm{SL}}$ to the value of A and B, the standard deviation of $\mathrm{SCL}_{\mathrm{SL}}$ and exp($B \times$ dist), which is referred to "term2," are calculated for different

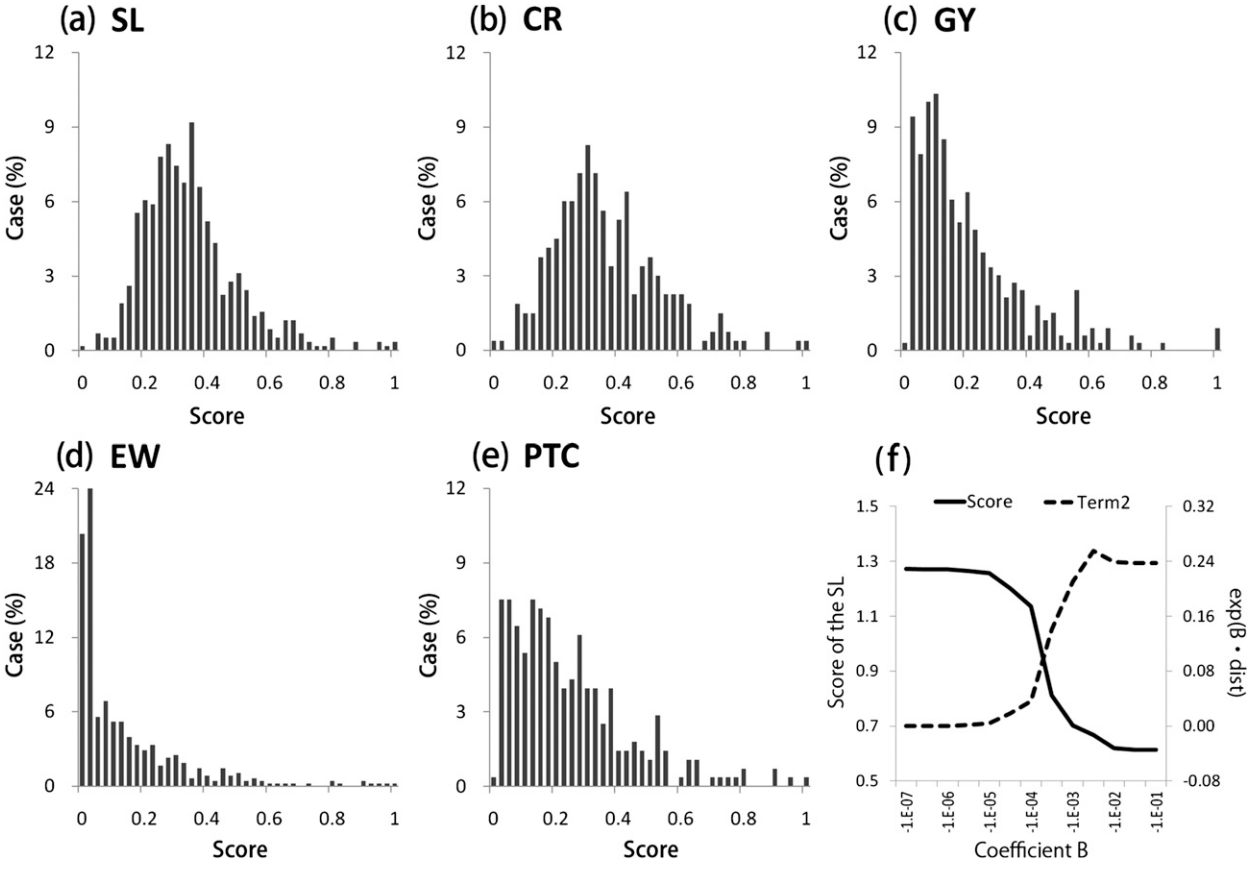

FIG. 3. Histograms of the percentage of cases against contribution score for the following flow patterns for TCG cases in the western North Pacific from 1979 to 2008: (a) SL, (b) CR, (c) GY, (d) EW, and (e) PTC. The horizontal axis is the contribution score ranging from 0 to 1. The vertical axis is the number of TCG cases as a percentage. (f) The property of coefficient B in a case of the SL; the horizontal axis is value of coefficient B, the left side vertical axis is standard deviations for SCR_{SL}, and the right side is the term of $\exp(B \times \text{dist})$.

B with $A = -1$, and plotted in the Fig. 3f. When the factor B is small, the standard deviation of score is large. That is, the score is distributed over a wide range. However, the standard deviation of term2 becomes smaller. Therefore, the factor B should be decided as a balance between score spreading and contribution from the distance parameter. Of course, the decided value is checked by consideration of consistency to the classification result by RH99, we decided factor B as -1.0×10^{-5} for the SL pattern. After this kind of tuning is done, the score distributions are widely spread for all 30-yr cases as shown in the histograms of Fig. 3.

g. *Validation of contributing flow patterns*

The flow pattern of the maximum contribution score is determined as the major flow pattern, but a subjective inspection of the meteorological field is conducted before a final decision is made. This is necessary to avoid misjudgments in particular situations. For example, if another TC exists near the TCG location 69 h before the time of TCG, the cyclonic flow associated with the first TC may form local wind shear that may result in a locally high score for SL and/or CR. However, this wind shear is not associated with the monsoon trough, and such cases should be removed. When the major contribution is denied by the subjective check, it is cast into the unclassified flow (UCF) pattern category. The UCF category contains cases where the major flow pattern cannot be determined by the objective algorithm in the present study and also includes cases where no value for the scores of any of the five patterns is computed for a TCG case. Such cases are seen in Table 1.

The second and the third contributing flow patterns are also ranked. For their minor contributions, however, we checked the statistical significance of the ranking using an f test and the Student's t test or Welch's t test. For each flow pattern, the relationship between neighboring ranks is checked at the 5% significance level using a t test. The results are shown in Table 2. From Table 2, the SL, CR, and PTC patterns show significant differences for the first (major)–second, and the second–third at the 5% significance level in the t test. The GY

TABLE 2. A statistical *t* test at the 5% significance level between ranking of contribution scores; "o" and "×" indicate "significant" and "not significant", respectively.

Patterns	First–second	Second–third	Third–fourth	Fourth–fifth
SL	o	o	×	×
CR	o	o	×	×
GY	o	o	×	×
EW	o	o	o	×
PTC	o	o	o	×

and EW patterns show a significant difference for the first–second, second–third, and third–fourth. In the following section, we will discuss the contribution of flow patterns confirmed by this significance test.

Typical cases of TCGs for the different major flow patterns are shown in Fig. 4 (the GY pattern is excluded here). The red star indicates the TCG location, and color shade represents zonal flow at 69 h before genesis time. Scores for each flow pattern are shown in the bar chart. In Fig. 4a, the shear line (blue dotted line) is detected near the genesis location by the objective algorithm. The SL score is the highest and thus determined as the major contribution pattern, and a secondary contribution from GY is present. In Fig. 4b, a confluence region represented by the yellow dotted line is detected at the leading edge of the westerly wind. There is also a preexisting TC about 1500 km to the west of the genesis location at the genesis time. In this case, CR provides the major and PTC the secondary contribution. TCG associated with the easterly wave trough is depicted in Fig. 4c. Each of the three green dotted lines represents part of the easterly wave trough as detected by the objective algorithm, but no score was computed for other flow patterns. In Fig. 4d, both a preexisting TC (purple star) and easterly wave troughs (green dots) are detected by the algorithm. According to the calculated contribution scores, PTC is the major and EW the secondary contributing flow pattern.

4. Results

a. Percent occurrence of the major contributing flow patterns

Table 3 shows the number (and percentage) of TCGs categorized as the major contribution into each of the five patterns for all TCG cases during the period from

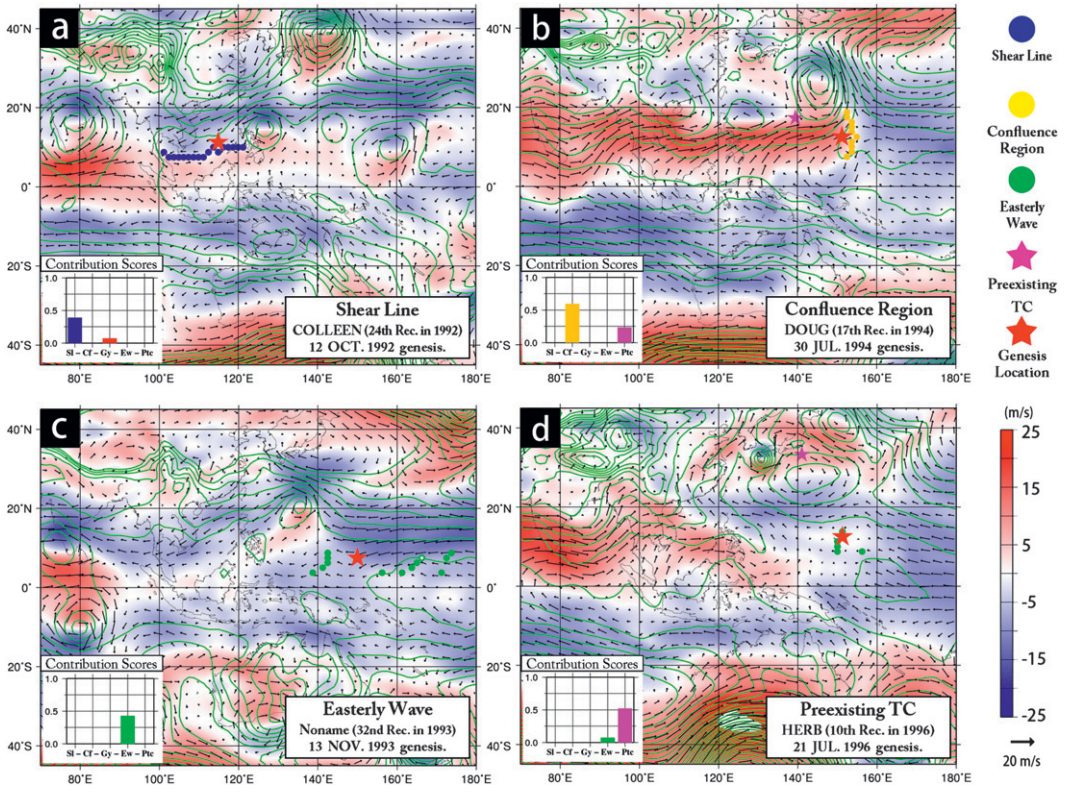

FIG. 4. Examples of flow patterns: (a) SL, (b) CR, (c) EW, and (d) PTC. The GY pattern is not shown. Vectors are the horizontal wind field at 850-hPa height, and the color shade is the zonal wind at the same height. Green color contours represent sea level pressure.

TABLE 3. Statistical summary of five flow pattern categories associated with TCG for the 30-yr study period from 1979 to 2008 and resampled to RH99 in the western North Pacific.

	ALL	SL (%)	CR (%)	GY (%)	EW (%)	PTC (%)	UCF (%)
Current (1979–2008)	908	380 (42)	146 (16)	59 (6)	165 (18)	97 (11)	61 (7)
Avg lat (°N)	12.9	12.1	14.0	12.5	13.0	12.8	15.9
Avg lon (°E)	143.4	142.5	140.2	139.5	145.0	154.0	139.0
Current (1984–92)*	217	89 (42)	32 (15)	18 (8)	42 (20)	33 (15)	—
RH99 (1984–92)*	199	84 (42)	58 (29)	5 (3)	36 (18)	16 (8)	—

* 1989 is excluded.

1979 to 2008. The most frequent pattern is SL at 42% of TCG cases, followed by CR and EW at 16% and 18%, respectively. The contribution from PTC and GY are 11% and 6%, respectively, indicating that these are rather minor flow patterns for TCG over the WNP. The UCF pattern, which accounts for 7% of all cases, includes both cases that did not have scores for any of the five patterns (4%) and those for which the objectively determined pattern was denied by subjective inspection of the meteorological chart (3%).

The geographic distribution of each pattern is shown in Table 3 and Fig. 5. The tabulated values are averaged over all of the cases of each pattern and the figure shows box plots for the distribution range of TCG latitude and longitude. The TCG locations are mainly concentrated at 12°N, 144°E. There is no significant difference in the TCG location among the five patterns, except for the PTC pattern. TCGs associated with the PTC occurred on average farther to the east of the other patterns with a 5% level of significance. The TCG location of the UCF pattern is biased to the north and west compared with the other classified patterns.

In the lower half of Table 3, the categorization results of the current study and RH99 are compared. Since the analysis period used by RH99 was from 1984 to 1992 except 1989, our results are resampled over the same period. According to the JTWC best-track data, there were 229 TCG cases in this period over the WNP. RH99 categorized 199 of these cases into the five patterns, while we categorized 217 cases. In both analyses SL is the most frequent pattern. CR and EW follow with around 20%, then PTC and GY have minor frequency. Thus, we estimate basically similar statistics compared with the previous study, despite a slight difference of numbers.

b. Temporal changes of the TC genesis environment

Figure 6 shows seasonal changes in the proportion of major flow patterns for the five classified and one unclassified patterns. Figure 6a shows the total number of cases in each pattern for each month over the analysis period from 1979 to 2008, and Fig. 6b shows the number of cases in each pattern for each month as a percentage of the monthly total. From Fig. 6a, TCG associated with the SL and EW patterns occurs throughout the year, although fewer cases occur in winter. The seasonal change of the EW pattern is less significant than the corresponding change in the SL pattern. From Fig. 6b, the SL pattern occurs in all months. When TCG occurs during winter and in the SL pattern, westerly winds do not extend from India. Rather, westerly winds exist locally over the WNP. This is discussed in section 5b again.

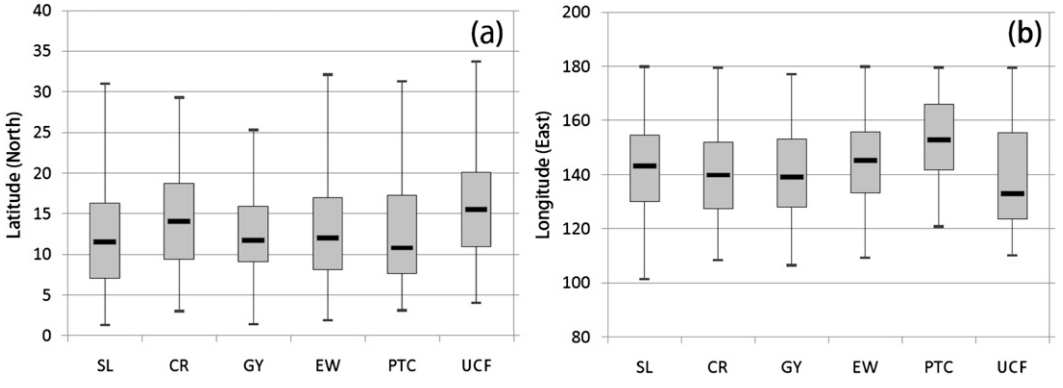

FIG. 5. Boxplots of tropical cyclone genesis location for all five flow patterns: (a) latitude and (b) longitude. The vertical bar shows the full range of the distributions, and the box shows the interquantile range of 25%–75% of all cases. The bold horizontal line indicates the median.

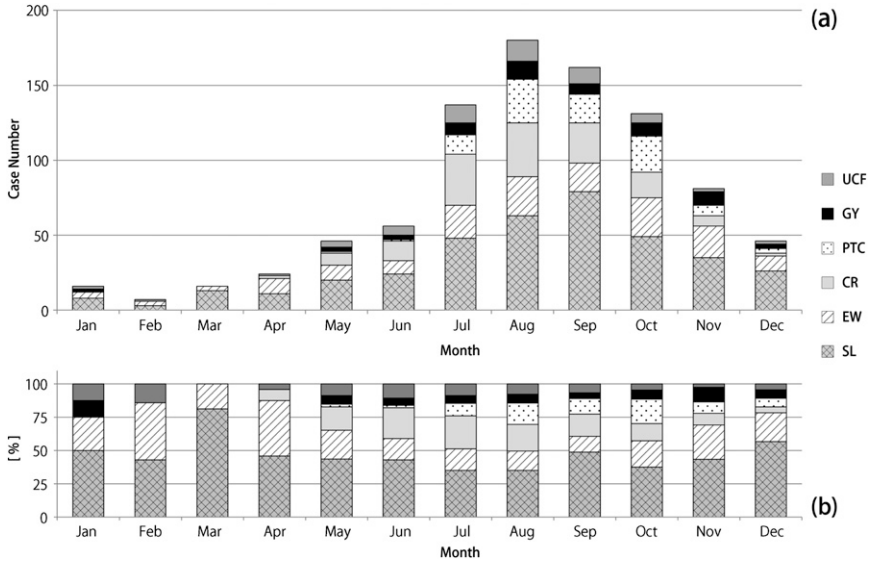

FIG. 6. Seasonal variation of the five flow patterns from 1979 to 2008 (30 yr): (a) accumulated number of TCG cases per month and (b) percentages normalized by the monthly total.

On the other hand, the CR and PTC patterns do not appear from January to March. The occurrence of CR and PTC cases increases in summer, and the proportion of CR is larger than that of EW in June, July, August, and September. These variations can be explained via the following consideration. The southwesterly wind tends to be stronger over the WNP in summer, thus the SL and CR flow patterns may be organized more frequently. Therefore, many TCs are generated in monsoon-related flow patterns such as SL and CR. Moreover, in summer, the number of TCs increases, and hence the opportunity for preparing the PTC flow pattern increases, thus TCG cases associated with PTC increase. The UCF pattern occurs in all seasons, and the number of UCF cases increases in summer.

Figure 7 shows the interannual change in the total number of TCG cases (Fig. 7a) and the percent occurrence (Fig. 7b) of the major flow pattern. Although SL is the dominant flow pattern for TCG overall, in 1995 the proportion of SL events was smaller than those of EW and PTC. In recent years from 2002 to 2007, the SL pattern has been especially dominant, and more than 50% of TCs were organized associated with the SL pattern in these years. The number of SL events seems to be increasing during the period from 1979 to 2008, and the calculated linear rate of increase is 1.3 $(10\ \text{yr})^{-1}$.

The next-most frequent patterns during the 30-yr analysis period are EW and CR. The TCG occurrence of these patterns shows significant interannual variability, ranging from a few percent to one-quarter of cases in a given year. The proportion of PTC events only accounts for 11% of TCG in the 30-yr analysis period (Table 3), yet contributed to more than 25% of TCGs in 1992, 1995, 1996, and 1997. Likewise, the GY pattern accounts for a low proportion of TCGs over the 30 years, but made a nonnegligible contribution in some years.

The black line at the top of Fig. 7 is the Niño-3 index, which is a proxy for the interannual variation of ENSO. The values are calculated by the Japan Meteorological Agency and are subject to a 5-month running mean. There is no significant correlation between the index and the frequency of each TCG pattern. However, the EW pattern has a correlation coefficient of −0.53 with 1% significance. This small but significant correlation is attributed to the relation between the easterly trade winds and ENSO. During a La Niña, easterly winds are enhanced, so that the possibility of EW pattern increases. The opposite occurs during an El Niño.

c. *The upper-tropospheric environment related to TCG*

The condition of the upper troposphere is important for TCG, and Gray (1968, 1998) suggests that weak vertical shear of horizontal wind and anticyclonic circulation at the upper levels of the troposphere are preferred for TCG. Thus, RH99 also considered the upper troposphere conditions in order to assess the flow patterns. Following them, we calculated ''circulation'' at 200 hPa and ''deep vertical shear of horizontal wind speed'' (200–850 hPa at the TCG location) using the horizontal wind field of JRA-25/JCDAS to diagnose the upper-tropospheric environment. The circulation is

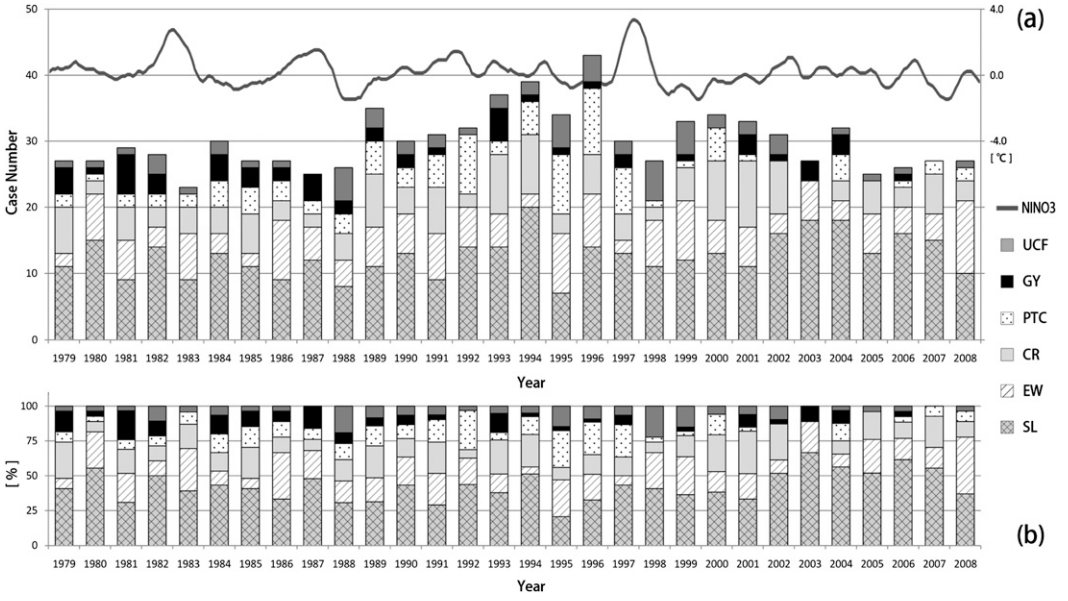

FIG. 7. Interannual variations of the five flow patterns: (a) accumulated number of TCG cases per year and (b) percentages normalized by the yearly number of TCG cases. A black line in (a) shows the Niño-3 index, which is taken during a 5-month running mean.

calculated along a circle approximately 1387 km in diameter (10 grid cells width of the reanalysis data), and centered at the TCG location. The vertical shear (VS) is calculated by $VS = |\mathbf{U}_{200} - \mathbf{U}_{850}|$ mean component of the horizontal wind at 200 and 850 hPa, respectively. Here **U** means zonal wind component. We will focus on the vertical shear produced by dominant flow over the WNP (i.e., trade easterly and monsoon westerly).

Figure 8 shows the intensity of circulation and vertical shear for all TCG cases in the analysis period. A positive circulation value indicates cyclonic circulation, and a negative value indicates anticyclonic circulation in Fig. 8a. About 75% of the classified TCGs occurred when the upper-tropospheric circulation was anticyclonic. However, there was no difference in upper circulation between the different flow patterns. Thus, anticyclonic circulation in the upper troposphere is the preferred condition for TCG in association with any lower-tropospheric flow pattern, which is consistent with Gray (1968, 1998).

From Fig. 8b, TCGs tend to occur under weak vertical shear for all five patterns, and more than 75% of TCG cases occurred when vertical shear was below 20 m s^{-1}. According to Gray (1968, 1998), weak vertical shear is a preferred condition for TCG, and tropical storms do not

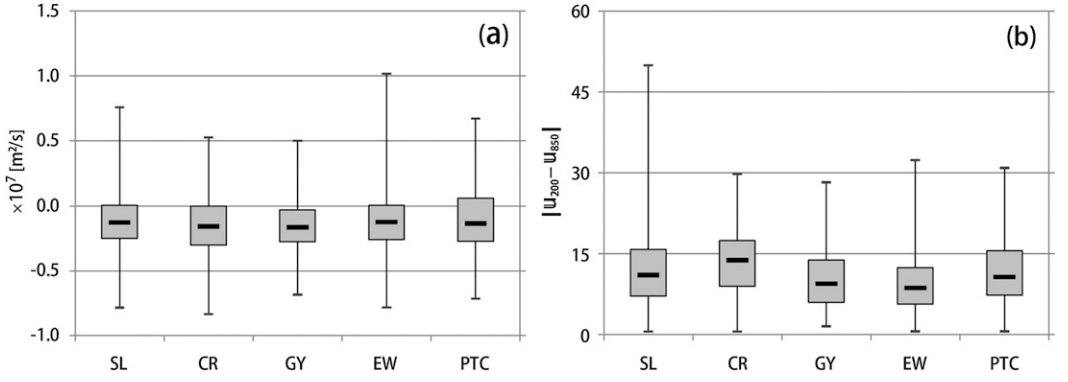

FIG. 8. Boxplots of (a) upper-tropospheric circulation and (b) deep vertical wind shear for all five flow patterns. The vertical bar shows the full range of the distributions, and the box shows the interquantile range of 25%–75% of all cases. The bold horizontal line indicates the median. A positive value of circulation indicates cyclonic circulation, and a negative value anticyclonic circulation.

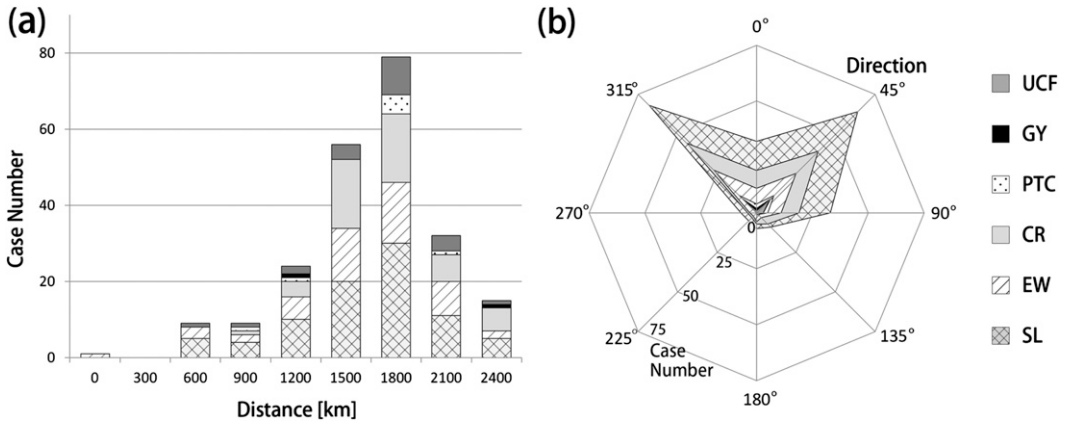

FIG. 9. Locations of an upper-tropospheric cyclonic circulation for all the TCG cases: (a) distance from the TCG location to the circulation and (b) direction toward the circulation; 0° (180°) is northward (southward). The case numbers in both panels are accumulated about upper 75th percentile cases for 30 yr from 1979 to 2008.

occur where the observed climatological tropospheric wind shear is large (i.e., greater than 20 m s^{-1}). Thus, the preference for weak vertical shear as a condition for TCG is consistent with previous studies, and is common among the five flow patterns.

Montgomery and Farrell (1993), Molinari et al. (1995), and Ferreira and Schubert (1999) suggested that the existence of the tropical upper tropospheric trough (TUTT) is a favorable condition for the TCG. Briegel and Frank (1997) concluded that approximately 40% of TCG cases formed when the TUTT was located within 2500 km to the northwest of the TCG location prior to genesis. This feature is also shortly checked for our 30-yr cases. We calculated circulation at 200 hPa at every grids for every TCG cases in the square domain (21×21 grids in 1.25°) centering each TCG location. The circulation is calculated by the way mentioned above in this section. The location that has the maximum cyclonic circulation in the domain is assumed as the location of the TUTT.

Figure 9 shows distance (Fig. 9a) and direction (Fig. 9b) of upper-tropospheric cyclonic circulation from the TCG location. Cases greater than circulation intensity equal to 0.72×10^{-7} (m^2 s^{-1}), which is the 75th percentile, are plotted. From Fig. 9a, the distance has a peak at approximately 1800 km. More than a half of the total TCG cases located within the 1800-km distance from the upper-tropospheric cyclonic circulation. This feature is consistent with Briegel and Frank (1997), and there is no significant difference among major flow patterns. It is obvious that many TCG cases take place when the upper-tropospheric cyclonic circulation is at the northwest of the TCG. While this is consistent with Briegel and Frank (1997), cyclonic circulations appear also at the northeast of the TCG location.

5. Discussion

a. Distributions of scores and relationships between patterns

In previous studies, each TCG was related to a single flow pattern (RH99; L08). In some TCG cases, however, multiple flow patterns may contribute to the genesis. Since five contribution scores are computed in this study, it is possible to estimate the contribution from different flow patterns. Figure 10 shows scatter diagrams of the contribution scores for combinations of major and minor flow patterns with a 5% significance level. The GY-major combinations were not included since there was no significant relation to other minor patterns. Figure 10a is, for example, a scatter diagram of SL (major contribution) and CR (minor contribution). The first-order regression line (FOR) and determination coefficient (represented by R^2) are also shown in each diagram. The FOR slope represents the change in the minor contribution score when the major contribution score is increasing. If the slope is steep, a minor pattern makes a greater contribution to the TCG case. In cases when the significance is less than the 5% criteria (see section 3), the plot is not shown (i.e., SL is considered until it is the third contribution, CR the third, PTC the third, and EW the fourth; see Table 2).

As seen in Fig. 10, there are many cases in which the score of the minor contribution pattern is close to that of the major. That is, the minor contribution patterns are also important features for such a TCG. The physical process of TCG may be different in which the combination of minor and major patterns varies, because the environmental flow features or the source of vorticity are different in each combination.

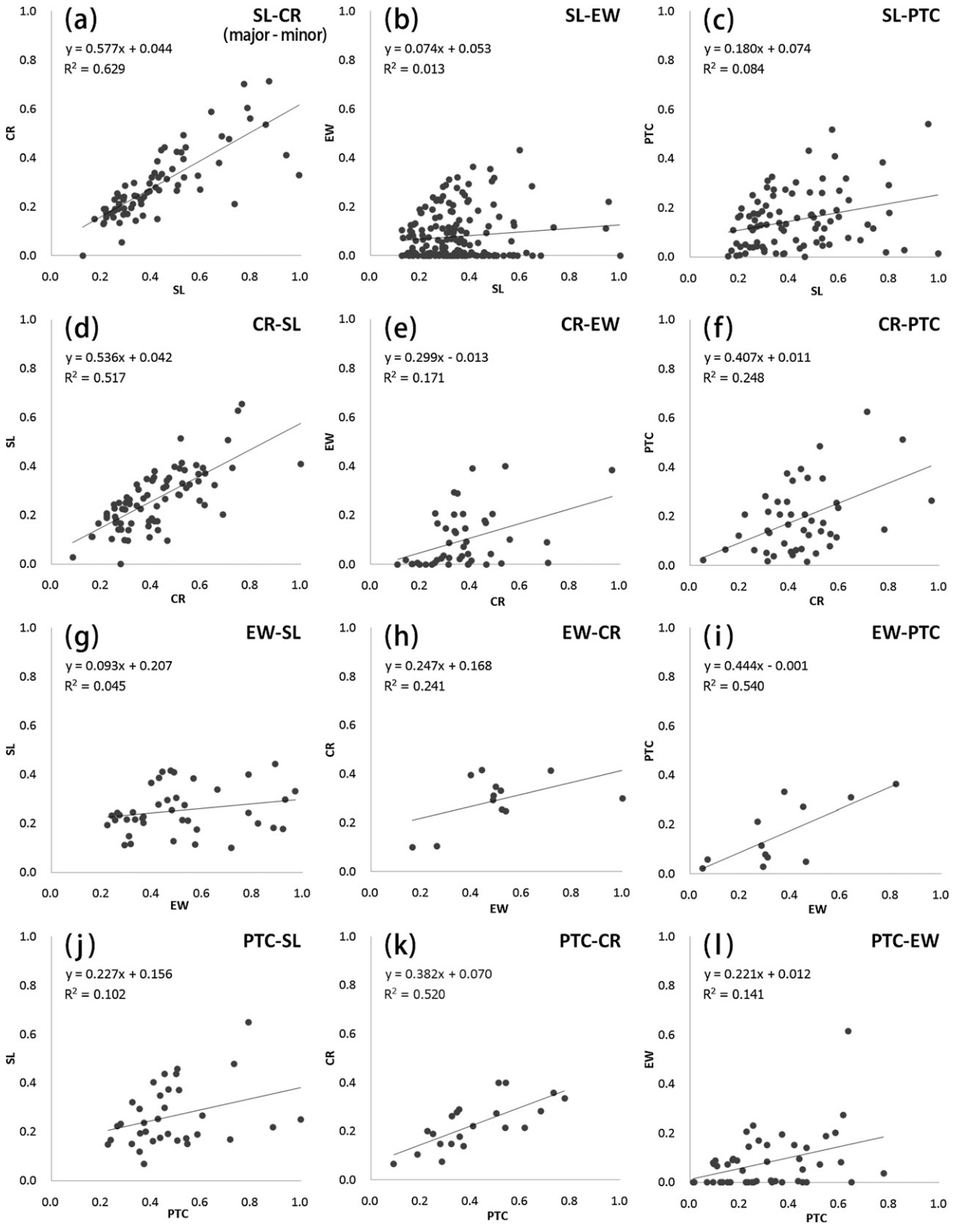

FIG. 10. Scatter diagrams of the major pattern scores vs minor pattern scores. The abscissa axis is the major score and the ordinate axis is the minor score. For SL, CR, and PTC, the minor score comprises the second and third contributions. For EW, the minor score includes the second, third, and fourth contribution. The line and R^2 value in each diagram are the first-order regression and determination coefficient, respectively.

First, we will discuss the SL and CR patterns. In Fig. 10a, the SL major pattern has a high correlation with CR, and the slope of the FOR is steeper than for other cases. In Fig. 10d, CR is the major pattern and also has a high correlation and a steeper slope with SL. This implies that the SL and CR patterns are highly correlated. This is a reasonable result since the SL and CR patterns appear at the northern flank and the eastern edge of the monsoon southwesterly winds, respectively.

The EW pattern does not have a high correlation with SL or CR, and the FOR slopes are less steep in Figs. 10b,e,g,h than others. This implies that the EW pattern is independent of SL and CR, which is consistent with the finding of L08 that TCG associated with the EW pattern are distinguished from those of monsoon-related patterns such as SL and CR. The independent nature of the EW pattern is more clearly seen from the following analysis. We counted the number of TCGs with a score from only one pattern (i.e., the scores of other patterns are zero). When EW is the major pattern (165 cases), the scores of the other patterns were all zero in 100 cases (61%). For cases where the other patterns are the major contribution, the ratios are 15% for SL, 15% for CR, and 16% for PTC. Thus, EW pattern tends to generate TC by itself. As an exception to this, the EW (major pattern) has a high correlation with PTC as show in Fig. 10i. The slope is relatively steeper, and the correlation is higher. Thus, it seems that EW has a certain relationship with PTC. One possibility is that PTC feeds vorticity into the TCG environment, and promotes evolution of tropical cyclones from the disturbance of the easterly wave.

Finally, we discuss the case when PTC is the major contributing pattern. The PTC pattern does not have a high correlation with SL and EW as seen in Figs. 10j,l. In addition, the FOR slopes in Figs. 10j,l are relatively gentle. So although PTC helps create a suitable TCG environment, SL or EW do not coexist when PTC is the major flow feature. On the other hand, PTC has a high correlation with CR and a relatively steep FOR slope in Fig. 10k. In the reverse case when CR is the major pattern (Fig. 10f), PTC also has a relatively high correlation and steeper slope. Therefore, the PTC and CR patterns tend to coexist. According to Li and Fu (2006), TCs that have a Rossby wave train do not always lead to new TC genesis. Thus, TCG in the PTC pattern requires some other background conditions. From the relationship mentioned above, the CR pattern may be considered as a candidate for the preferred condition for TCG in a PTC major pattern.

b. The background environment of the flow patterns

It is interesting to see the current result from the genesis potential index (GPI) as the background environment of five flow patterns. We have calculated the GPI as defined by Emanuel and Nolan (2004):

$$\mathrm{GPI} = |10^5\eta|^{1.5}\left(\frac{H}{50}\right)^3\left(\frac{V_{\mathrm{pot}}}{70}\right)^3(1+0.1V_{\mathrm{shear}})^{-2}, \qquad (7)$$

where η is the absolute vorticity at 850 hPa, H is the relative humidity at 700 hPa, and V_{shear} is the magnitude of the vertical shear of horizontal wind between 850 and 200 hPa. The potential intensity V_{pot} is calculated by using a FORTRAN routine provided by Dr. Emanuel (http://eaps4.mit.edu/faculty/Emanuel/products). Hereafter, we refer the term of $|10^5\eta|^{1.5}$ as the vorticity (VOR) term, $(H/50)^3$ as the relative humidity (RH) term, $(V_{\mathrm{pot}}/70)^3$ as the potential intensity (PI) term, and $(1 + 0.1V_{\mathrm{shear}})^{-2}$ as the vertical shear (VS) term. The GPI is also calculated using JRA/JCDAS reanalysis data. According to the distribution of the TCG location shown in Fig. 5, an averaging domain is defined to be from 100° to 180° in longitude and from 0° to 35° in latitude.

The distribution of calculated GPI and TCG locations for the SL-, EW-, and CR-major patterns are shown in Fig. 11, where TCG locations during SL-, EW-, and CR-major cases in July–October (JASO) are plotted using different symbols and the spatial distribution of GPI values averaged over the same period is defined by the background shading. It is seen that the distribution of plots follows the shape of high GPI values though there are considerable plots to the south of 10°N where GPI values are relatively low.

Figure 12a shows seasonal changes of the GPI and the major five patterns averaged over the 30 yr. The correlation coefficients between major five patterns and the GPI (or equation terms) are shown in Table 4. The correlation coefficients with GPI exceed 0.89 for all five patterns. This consistency of seasonal changes can be found in Fig. 12a. In the five patterns, the SL- and CR-major patterns have especially strong correlation; these coexistences are more than 0.94. However, there are differences in correction intensity between terms of the GPI equation. For example, when the SL is major flow pattern, the score has stronger correlation with the PI term than RH or VS. The EW pattern also has same correlation with the SL pattern. But, the CR pattern has a stronger correlation with the RH term than the PI. This difference seems to come from the difference of the seasonal peak. The frequency peak of the SL or EW pattern exists around August to October, but the CR pattern is frequent from July to August. In the GPI terms, the PI term has the higher values from August to October, and the RH and VS terms are high from July to August.

According to Murakami et al. (2011), the PI is one of the factors causing an increase in GPI for the entire

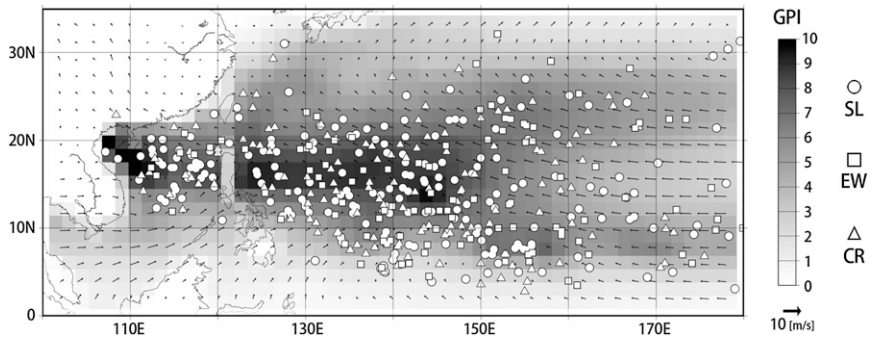

FIG. 11. Horizontal distribution of TCG locations and the corresponding GPI distribution for JASO averaged over 30 yr. Circles, squares, and triangles are TCG locations of SL-, EW- and CR-major patterns, respectively.

WNP, and CAPE is the largest contributor to the increase in PI. Because CAPE can be determined mainly by sea surface temperature, the TCG cases of the SL or EW pattern would be controlled by the seasonal change of sea surface temperature. On the other hand, the CR pattern is related with the monsoon trough as mentioned in the above section. According to Wu et al. (2012), when the monsoon trough is strong, convection is enhanced, relative humidity is increased, and vertical shear of zonal wind is reduced. All these conditions are favorable for TCG, and the number of CR pattern cases would increase according to intensification of such favorable environments.

Figure 12b shows interannual changes of GPI and the EW patterns. The correlation coefficients between the five flow patterns and GPI (or equation terms) are shown in Table 4. It is clear that every major flow pattern has weak correlation with the GPI. Menkes et al. (2012) pointed that the GPI is able to reproduce interannual changes over the North Atlantic, but is not able to reproduce that over the WNP. The SL and CR patterns seem to have a little better correlation, but the EW has a weak correlation coefficient of 0.083. For the PTC pattern, the correlation coefficient is negative. Since the GPI is a potential for the TCG, a negative correlation is not useful. The GPI is originally designed for seasonal

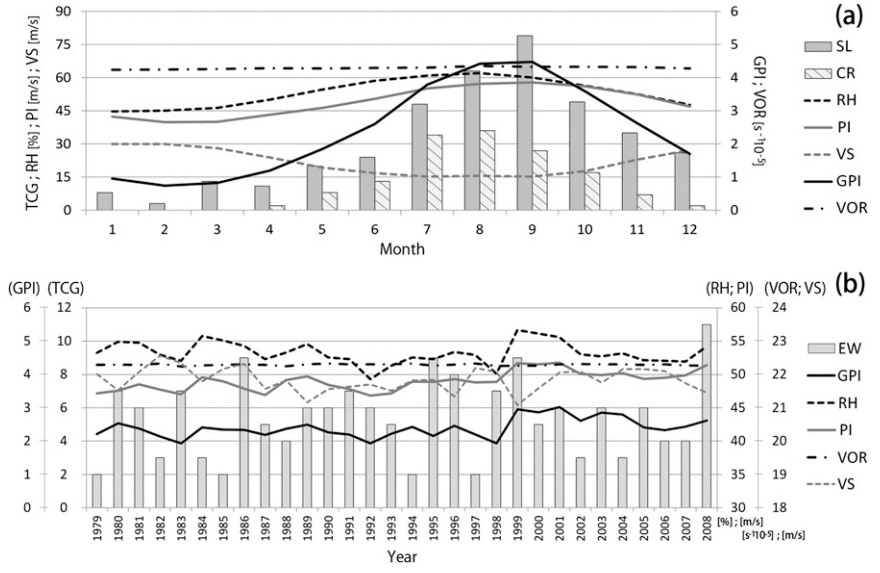

FIG. 12. Comparison with the GPI: (a) seasonal variation; the accumulated number per one month of the SL or CR patterns for 30 yr from 1979 to 2008. The values of GPI and its terms are averaged among 30 yr (1 month)$^{-1}$. (b) Interannual variation; the accumulated number per one year of the EW patterns for 30 yr. The values of the GPI and its terms are averaged among 1 yr.

TABLE 4. Correlation coefficients between seasonal/interannual changes of GPI and major flow patterns for the 30-yr cases. VOR, RH, PI, and VS are terms of the GPI equation.

Seasonal changes					
Patterns	GPI	VOR	RH	PI	VS
SL	0.96	0.88	0.83	0.94	−0.80
CR	0.94	0.80	0.92	0.87	−0.88
GY	0.89	0.86	0.76	0.92	−0.71
EW	0.90	0.92	0.79	0.93	−0.77
PTC	0.89	0.84	0.73	0.86	−0.70
All	0.98	0.90	0.88	0.96	−0.84

Interannual changes					
Patterns	GPI	VOR	RH	PI	VS
SL	0.31	0.56	−0.16	0.13	−0.02
CR	0.29	0.17	0.29	0.27	−0.16
GY	0.04	0.25	0.24	−0.24	0.13
EW	0.08	−0.41	0.07	0.15	−0.41
PTC	−0.27	0.07	−0.13	−0.15	−0.22
All	0.25	0.30	0.11	0.22	−0.47

change, so there will be some difficulties in application to interannual change.

It is also of interest to determine the role of the Madden–Julian oscillation (MJO; Madden and Julian 1994) on TCG since the location of the westerly burst relates with MJO as reported by Wheeler and Hendon (2004) and Maharaj and Wheeler (2005). Taniguchi et al. (2010) have previously reported a TCG case associated with the westerly winds of the MJO. To show the relation, the MJO index of Wheeler and Hendon (2004) is plotted for the SL and CR pattern cases, which are the most likely to be affected by MJO. In the summer season (July–October) 55% of SL cases occurred when the MJO is active (amplitude > 1), among which 49% are in phases 5–7 (active in WNP). For the CR pattern, the percentages are 57% and 60%, respectively. In the winter season (December–February), 62% of SL occurred with active MJO, among which 52% are in phases 5–7.

These results suggest that the MJO contributes to the TC genesis to some extent, but other factors are important to TCG since nearly two-thirds of TCG are not directly affected by the MJO.

c. *The unclassified flow pattern*

In this section, we briefly examine TCG cases categorized into the unclassified flow (UCF) pattern. We show four examples of typical UCF in Fig. 13 from the 36 cases that have no scores for the five flow patterns of interest. The location of TCG is represented by a red star in each diagram. Figure 13a shows the fourth TCG

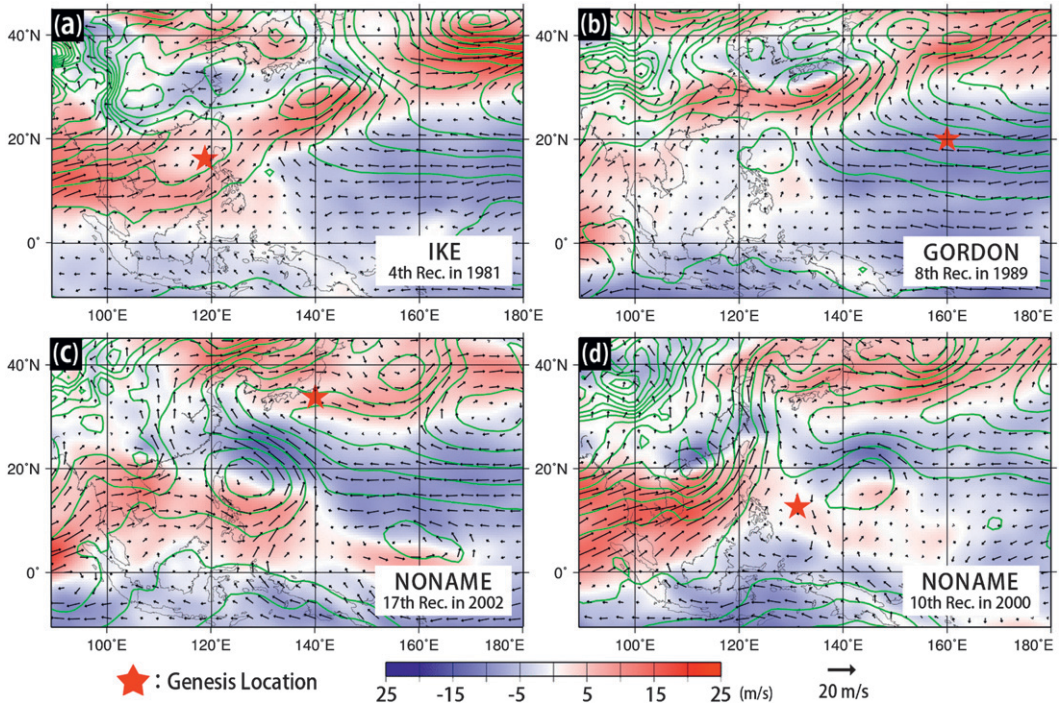

FIG. 13. Examples of unclassified flow patterns. A red star represents the location of cyclogenesis in each diagram. Vectors are the horizontal wind field at 850-hPa height and the color shade is the zonal wind at the same height. Green color contours represent sea level pressure.

record in 1981 in JTWC, which was generated in the South China Sea. Eight cases of this type of TCG were identified, and all were generated in westerly winds, and no contribution from SL, CR, or EW can be expected.

Figure 13b shows the eighth record in 1989, which was generated in an eastern area of the WNP. There are 13 cases of this type, and these are widely distributed from latitudes 4.0°–29.5°N. Almost all such TCG cases occurred in easterly winds, but a few cases that are generated in higher latitudes occurred in westerly winds.

Figure 13c shows the 17th record in 2002, for which the TCG latitude is the highest of all 908 cases at 33.7°N. Four of the unclassified cases were generated near Japan, and the TCG latitudes of other three cases are 24.6°, 28.0° and 30.4°N.

The remaining 10 UCF cases were generated in the typical TCG area to the east of the Philippines, but no remarkable flow features are identified. The wind speed is low in either a westerly or easterly direction as seen in Fig. 13d, which is the 10th record in 2000.

6. Summary

In this study, we carried out categorization of flow features of the lower troposphere associated with TCG over the western North Pacific (WNP). The five patterns identified are monsoon shear line (SL), monsoon confluence region (CR), monsoon gyre (GY), easterly wind wave (EW), and preexisting tropical cyclone (PTC), and are based on those of RH99. We extended the analysis period to 30 yr from 1979 to 2008, which includes the whole period of RH99. In the present study, the categorization was carried out objectively by using a new method of calculating contribution scores from JRA-25/JCDAS reanalysis data. The scores indicate the magnitude of the contribution of each flow pattern to the TCG, and are calculated for all 908 TCG cases. The major contributing flow pattern for each TCG is identified as the flow pattern with the highest contribution score. From the categorization results, it is clear that the SL pattern is the most frequent flow pattern, followed by the CR and EW patterns. PTC is a less frequent pattern, and there are very few TCG cases associated with the GY pattern. These results are consistent with those of RH99.

We also considered the seasonality of the major contributing flow pattern. The SL pattern is the most frequent flow pattern throughout the year. The EW pattern also occurs throughout the year although its ratio to other patterns decreases in summer. The CR and PTC patterns occur as major contributing flow patterns in summer only. The interannual change of flow patterns over the 30-yr study period is also investigated. The order of the occurrence frequency of the five patterns does not change dramatically for the longer period from 1979 to 2008 compared to that of RH99. Interannual change of EW pattern seems to have relationships with ENSO. In addition, the proportion of TCG cases associated with the SL pattern slightly increases in the 6 yr from 2002 to 2007.

The upper-tropospheric circulation and deep vertical wind shear during TCG were also investigated. TCG occurs when there is anticyclonic circulation in the upper troposphere for 75% of cases, and this result does not differ among the five patterns. In regards to the vertical shear of horizontal wind, weaker shear is the preferred condition for TCG, and there is not a large difference among the five flow patterns. These results are consistent with previous findings (Gray 1968, 1998).

In the previous studies (RH99; L08), each TCG is related to a single flow pattern although TCs often appear to be generated in an environment organized by multiple flow patterns. Thus, we investigate interpattern relationships and the preferred combinations of flow patterns. To do so, we examine correlations between scores of the major and secondary contributions. The contribution scores of SL, CR, and GY patterns have a good correlation with each other. Thus, the background condition generating these flow patterns is common, and is considered to be the monsoon trough elongated toward the WNP in the Northern Hemisphere summer. On the other hand, the EW pattern does not have much correlation with the other flow patterns, and tends to occur as an independent major flow pattern. For the PTC pattern, there is a relatively high correlation with the CR flow pattern.

Acknowledgments. The authors thank Drs. Tetsuya Takemi, Wataru Yanase, and Yoshiyuki Kajikawa for valuable discussions and the anonymous reviewers for their constructive comments. This work was performed using the best-track data of Joint Typhoon Research Center, JRA-25/JCDAS reanalysis data of the Japan Meteorological Agency (JMA), and the Niño-3 index of the JMA.

REFERENCES

Briegel, L. M., and W. M. Frank, 1997: Large-scale influences on tropical cyclogenesis in the western North Pacific. *Mon. Wea. Rev.,* **125,** 1397–1413.

Chen, S. S., R. A. Houze Jr., and B. E. Mapes, 1996: Multiscale variability of deep convection in relation to large-scale circulation in TOGA COARE. *J. Atmos. Sci.,* **53,** 1380–1409.

Chen, T. C., S. Y. Wang, M. C. Yen, and A. J. Clark, 2008: Are tropical cyclones less effectively formed by easterly waves in the western North Pacific than in the North Atlantic? *Mon. Wea. Rev.,* **136,** 4527–4540.

Emanuel, K. A., and D. S. Nolan, 2004: Tropical cyclone activity and global climate. Preprints, *26th Conf. on Hurricanes and Tropical Meteorology,* Miami, FL, Amer. Meteor. Soc., 10A.2. [Available online at https://ams.confex.com/ams/pdfpapers/75463.pdf.]

Ferreira, R. N., and W. H. Schubert, 1999: The role of tropical cyclones in the formation of tropical upper-tropospheric troughs. *J. Atmos. Sci.,* **56,** 2891–2907.

Gray, W. M., 1968: Global view of the origin of tropical disturbances and storms. *Mon. Wea. Rev.,* **96,** 669–700.

——, 1998: The formation of tropical cyclones. *Meteor. Atmos. Phys.,* **67,** 37–69.

Heta, Y., 1990: An analysis of tropical wind fields in relation to typhoon formation over the western Pacific. *J. Meteor. Soc. Japan,* **68,** 65–77.

——, 1991: The origin of tropical disturbances in the equatorial Pacific. *J. Meteor. Soc. Japan,* **69,** 337–351.

Holland, G. J., 1995: Scale interaction in the western Pacific monsoon. *Meteor. Atmos. Phys.,* **56,** 57–79.

Lander, M. A., 1994: Description of a monsoon gyre and its effects on the tropical cyclones in the western North Pacific during August 1991. *Wea. Forecasting,* **9,** 640–654.

Lee, C.-S., K. K. W. Cheung, J. S. N. Hui, and R. L. Elsberry 2008: Mesoscale features associated with tropical cyclone formations in the western North Pacific. *Mon. Wea. Rev.,* **136,** 2006–2022.

Li, T., and B. Fu, 2006: Tropical cyclogenesis associated with Rossby wave energy dispersion of a preexisting typhoon. Part I: Satellite data analyses. *J. Atmos. Sci.,* **63,** 1377–1389.

——, X. Ge, B. Wang, and Y. Zhu, 2006: Tropical cyclogenesis associated with Rossby wave energy dispersion of a preexisting typhoon. Part II: Numerical simulations. *J. Atmos. Sci.,* **63,** 1390–1409.

Madden, R. A., and P. R. Julian, 1994: Observations of the 40–50-day tropical oscillation—A review. *Mon. Wea. Rev.,* **122,** 814–837.

Maharaj, E. A., and M. C. Wheeler, 2005: Forecasting an index of the Madden-oscillation. *Int. J. Climatol.,* **25,** 1611–1618.

McDonald, N. R., 1998: The decay of cyclonic eddies by Rossby wave radiation. *J. Fluid Mech.,* **361,** 237–252.

Menkes, C. E., M. Lengaigne, P. Marchesiello, N. C. Jourdain, E. M. Vincent, J. Lefevre, F. Chauvin, and J. F. Royer, 2012: Comparison of tropical cyclogenesis indices on seasonal to interannual timescales. *Climate Dyn.,* **38**, 301–321, doi:10.1007/s00382-011-1126-x.

Molinari, J., S. Skubis, and D. Vollaro, 1995: External influences on hurricane intensity. Part III: Potential vorticity structure. *J. Atmos. Sci.,* **52,** 3593–3606.

Montgomery, M. T., and B. F. Farrell, 1993: Tropical cyclone formation. *J. Atmos. Sci.,* **50,** 285–310.

Murakami, H., B. Wang, and A. Kitoh, 2011: Future change of western North Pacific typhoons: Projection by a 20-km-mesh global atmospheric model. *J. Climate,* **24,** 1154–1169.

Onogi, K., and Coauthors, 2007: The JRA-25 Reanalysis. *J. Meteor. Soc. Japan,* **85,** 369–432.

Reed, R. J., and E. E. Recker, 1971: Structure and properties of synoptic-scale wave disturbances in the equatorial western Pacific. *J. Atmos. Sci.,* **28,** 1117–1133.

Ritchie, E. A., and G. J. Holland, 1999: Large-scale patterns associated with tropical cyclogenesis in the western Pacific. *Mon. Wea. Rev.,* **127,** 2027–2043.

Serra, L. Y., G. N. Kiladis, and M. F. Cronin, 2008: Horizontal and vertical structure of easterly waves in the Pacific ITCZ. *J. Atmos. Sci.,* **65,** 1266–1284.

Shapiro, L. J., 1977: Tropical storm formation from easterly waves: A criterion for development. *J. Atmos. Sci.,* **34,** 1007–1021.

Tam, C. Y., and T. Li, 2006: The origin and dispersion characteristics of the observed tropical summertime synoptic-scale waves over the western Pacific. *Mon. Wea. Rev.,* **134,** 1630–1646.

Taniguchi, M., W. Yanase, and M. Satoh, 2010: Ensemble simulation of cyclone Nargis by a global cloud-system-resolving model–modulation of cyclogenesis by the Madden-Julian Oscillation. *J. Meteor. Soc. Japan,* **88,** 571–591.

Wheeler, M. C., and H. H. Hendon, 2004: An all-season real-time multivariate MJO index: Development of an index for monitoring and prediction. *Mon. Wea. Rev.,* **132,** 1917–1932.

Wu, L., Z. Wen, R. Huang, and R. Wu, 2012: Possible linkage between the monsoon trough variability and the tropical cyclone activity over the western North Pacific. *Mon. Wea. Rev.,* **140,** 140–150.

Yanai, M., 1961: A detailed analysis of typhoon formation. *J. Meteor. Soc. Japan,* **39,** 187–214.

——, 1968: Evolution of a tropical disturbance in the Caribbean Sea region. *J. Meteor. Soc. Japan,* **46,** 85–109.

Zehr, R. M., 1992: Tropical cyclogenesis in the western North Pacific. NOAA Tech. Rep. NESDIS 61, 181 pp.